Proceedings of APMC2001, Taipei, Taiwan, R.O.C.

VBIC MODEL APPLICABILITY AND EXTRACTION PROCEDURE FOR InGaP/GaAs HBT

S.V. CHEREPKO and J.C.M HWANG
Lehigh University
5E Packer Av., Bethlehem PA, 18015 USA
E-mail: svcher@lehigh.edu and jh00@lehigh.edu

In this paper the applicability of VBIC-95 for InGaP/GaAs HBTs modelling is examined. Extraction procedure is presented for parameters responsible for saturation currents, thermal resistance, internal base resistance and forward transit time. Resulting VBIC model was verified against large-signal DC and AC measurements.

1 Introduction

The VBIC model for bipolar transistors [1] is an extension of the SPICE Gummel-Poon (SGP) model for Si bipolar transistors. Questions remain whether it is applicable to GaAs HBTs. Among the possible concerns are: 1) The thermal resistance of HBTs is often reported to be temperature dependent, which is not modeled by VBIC. 2) The ideality factors of base-collector and base-emitter current components in HBT were found to change with temperature, which are not modelled by VBIC. 3) Relatively light collector doping and relatively high operation current densities make HBTs very susceptible to the base push-out (Kirk) effect. It is not clear whether SGP-like formula for base transit time in VBIC can account for this effect. 4) Modulation of base-collector depletion capacitance by collector current is not modelled in VBIC. Furthermore, VBIC model extraction procedures published to date either deal with only DC or AC part of the model [2, 3], or rely on extensive use of numerical optimisation [4].

In this paper the extraction procedure of major VBIC model parameters is presented for InGaP/GaAs HBTs. Model applicability is verified throughout the extraction and by comparison with large signal DC and AC measurements. Transistors studied were single-heterojunction 3×20 μm single-emitter HBTs with base width of 0.1 μm, collector doping of 10^{16} cm^{-3}, and unity-gain frequency of 40 GHz.

2 Simplified VBIC model

The topology of VBIC model is shown in Fig. 1. Note that several parts of VBIC equivalent circuit are omitted in Fig. 1: thermal sub-circuit, excess phase delay sub-circuit, base-emitter and base-collector overlap capacitors and base-collector breakdown current source. The full model is complex and contains 86 parameters. However, specifics of HBT make it possible to consider a simplified version (Fig. 2). Transformation from VBIC to the simplified model is justified by the following: 1) The formulas derived for epi-layer resistance and charge (R_{CX} and Q_{BCX}) did not take into account the base push-out effect and therefore may be incorrect when Kirk effect occurs. In addition, there is no direct procedure known to extract the associated parameters. For these reasons both R_{CX} and Q_{BCX} can be dropped. 2) The HBT topology naturally calls for SGP-like separation of both DC and AC base-collector currents into internal and external components. This can be accomplished by connecting together the "substrate" and "collector" terminals in the VBIC model and using I_{CCP}, I_{BEP}, and Q_{BEP} to model the external base-collector current. 3) There is no parasitic *pnp* transistor in *npn* HBT, therefore I_{BCP}, Q_{BCP}, R_{BP}, and R_S can be eliminated. 4) Topologically, only non-ideal component of I_{BEX} may contribute to DC external base-emitter current in HBT. For DC current there is no significant difference whether it is internal or external since DC voltage drop across R_{BI} is typically small. The whole external base-emitter branch therefore can be eliminated. 5) For HBTs with ordered InGaP/GaAs base-emitter heterojunction forward and reverse transport currents should be equal for equal base-emitter and base-collector potentials. It means that the same set of parameters can be used

0-7803-7138-0/01/$10.00 ©2001 IEEE

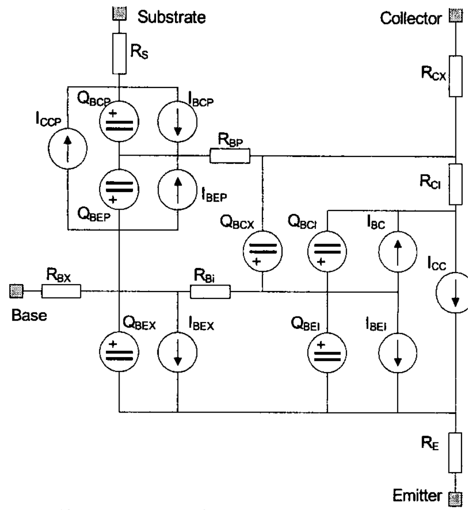

Fig. 1. VBIC model topology. Note: the thermal sub-circuit is not shown.

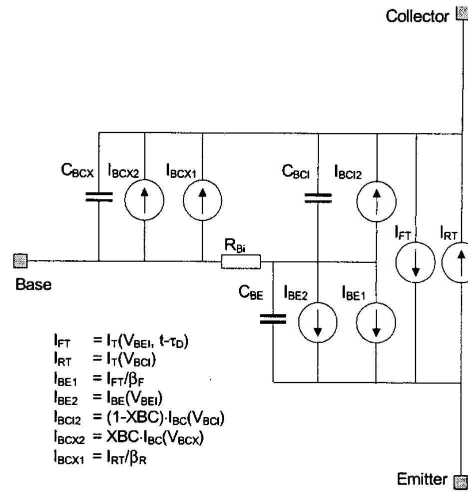

Fig. 2. Simplified SGP-like sub-model used for extraction.

for both of them. 6) The ideal component of base-emitter current mostly arises from bulk recombination and therefore can be modelled as forward transport current divided by forward current gain β_F. This current gain is assumed to be temperature-independent. 7) On the other hand, the ideal component of base-collector current is dominated by electron transport from external collector through external base directly to base contact. This is not very different from transport of electrons through internal base into emitter, which is essentially reverse transport current. The ideal component of base-collector current therefore can be modelled as a scaled reverse transport current. This scale is approximately equal to external/internal base ratio and for this reason is also assumed temperature-independent.

All DC current sources in the simplified model are defined in terms of three basic functions: $I_T(V)$, $I_{BE}(V)$ and $I_{BC}(V)$. They represent three primary conduction mechanisms: transport currents, and base-emitter and base-collector non-ideal currents, respectively. Each basic function has the same form as VBIC transport current sources:

$$I(V) = I_S e^{-\frac{qE_A}{N_0 k T_J}\left(1-\frac{T_J}{T_0}\right)} \left(e^{\frac{qV}{N_0(1+\alpha_N(T_J-T_0))kT_J}} - 1 \right), \tag{1}$$

where I_S,, E_A, N_0 and α_N are the parameters to be extracted (different for each basic function); V is the bias voltage; T_J is the internal temperature; T_0 is the reference temperature (VBIC model parameter *TNOM*), k is the Boltzmann constant; and q is the electron charge. Parameter $XBC = 0.35$ in the sub-model was estimated from geometry.

The AC part comprises capacitors C_{BE}, C_{BCX}, C_{BCI} and phase delay τ_D. All capacitors include depletion and diffusion contributions. Base-collector barrier capacitance is divided between internal and external parts using SGP-like parameter *XBC*.

3 DC parameters extraction

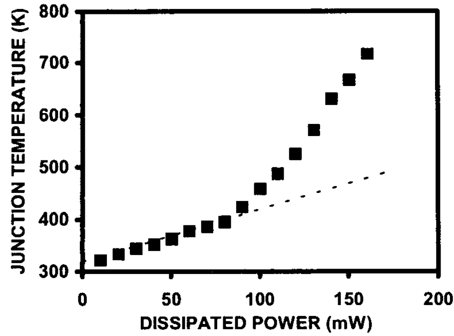

Fig. 3 Junction temperature vs. dissipated power. Ambient temperature 70°C.

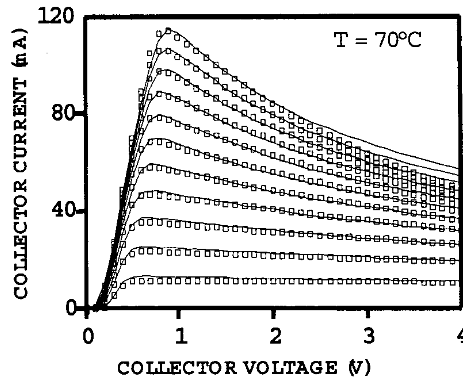

Fig. 4 (symbols) Measured vs. (lines) simulated *I-V* characteristics.
$I_B = 0.075, 0.15, \ldots, 0.875$ mA bottom top.

The parameters of basic functions $I_T(V)$, $I_{BE}(V)$ and $I_{BC}(V)$ were extracted using forward and reverse Gummel characteristics (FGC and RGC) measured at different temperatures. At each temperature, the saturation currents and ideality factors (I_{SAT} and n) for I_T, I_{BE}, and I_{BC} were extracted together with forward and reverse current gains β_F and β_R. This was done by first, extracting I_{SAT} and n for I_T using collector current of FGC. Then I_{SAT} and n for I_{BE} were extracted together with β_F by fitting log of base current of FGC to $\log(I_{BE}(V_{BE}) + I_T(V_{BE})/\beta_F)$. Finally, I_{SAT} and n for I_{BC} and β_R were extracted by fitting log of base current of RGC to $\log(I_{BC}(V_{BC}) + I_T(V_{BC})/\beta_R)$.

Temperature dependencies of I_{SAT} and n were then examined for each basic function to determine parameters I_S, E_A, N_0 and α_N. Ideality factors were first fitted with straight lines to obtain the N_{0xx} and α_{Nxx}. The pre-exponential factors (I_{Sxx}) and activation energies (E_{Axx}) were then extracted from Arrhenius plots of saturation currents. Forward and reverse current gains were just averaged over all temperatures.

Transition from sub-model back to VBIC is trivial for transport currents since they have exactly the same form as Equation (1). The rest of current sources in VBIC have α_N equal to zero. For them extracted activation energy E'_A was modified as follows: $E_A = E'_A - T_0 V^* \alpha_N$. This transformation makes the temperature response of Equation (1) with activation energy E'_A close to that with E_A and $\alpha_N = 0$ for biases close to V^*. Characteristic voltage V^* was selected as 1.3 and 1.1 V for base-emitter and base-collector currents, respectively. Note that while the non-ideal component of I_{BEP} was used to implement I_{BCX2}, the I_{BCX1} was implemented as I_{CCP}. This was done to account for base-collector diffusion charge.

Thermal resistance was extracted by measuring a series of constant power characteristics $I_C(V_{CE})$. For each power level P collector voltage V_{CE} was swept from 1.5 to 4 V and at each V_{CE} the base current was adjusted so that $I_C = P/V_{CE}$. The saturation current of I_T was extracted from $\ln(I_C)$ vs. V_{BEi} plot at each power level. Knowing dependence of saturation current on temperature (through parameters of I_T extracted earlier) the junction temperature was calculated and plotted vs. power (Fig. 3). From Fig. 3 it is clear that the thermal resistance is not constant. Since there is no way to implement this dependence in VBIC, a low-power value (dotted line in Fig. 3) was taken as the model parameter *RTH* in VBIC.

The extracted VBIC model was verified against measured *I-V* characteristics (Fig. 4).

4 AC parameters extraction

Parameters extracted in this section include internal base resistor (*RBI*), excess phase delay (*TD*), reverse transit time (*TR*) and those responsible for bias dependence of forward transit time (*TF*, *ITF*, *XTF*). All of them (except for TR) were extracted from small-signal S-parameters measured in active regime. Fig. 5 shows the small-signal equivalent circuit of the simplified model. First, Z_{BI} was extracted at small I_C (before onset of base push-out) using known X_{BC}. At each frequency R_{BI} was calculated according to:

$$R_{BI} = \mathrm{Re}\left(\frac{Y_{11} + Y_{21} + X_{BC}(Y_{12} + Y_{22})}{(Y_{11}Y_{22} - Y_{12}Y_{21})(1 - X_{BC})} \cdot \frac{Y_{12} + Y_{22}}{Y_{11} + Y_{21}} \right), \tag{2}$$

where Y_{ij} are Y-parameters calculated after de-embedding all external elements. The value of R_{BI} was then averaged over all frequencies. At high I_C the value of X_{BC} may change (decrease) because of two-dimensional distribution of pushed-out holes in collector. On the other hand, R_{BI} is not expected to vary with bias because of very high base doping. The R_{BI} extracted at small I_C was therefore used to calculate G_{BE} and G_T at all biases and frequencies according to:

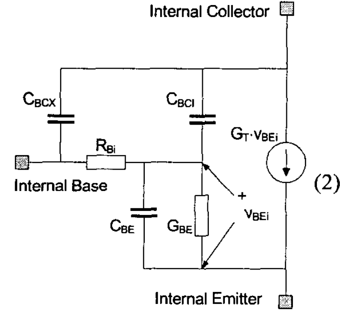

Fig. 5. Small signal equivalent circuit of sub-model in active regime.

$$G_T = A \cdot (Y_{21} - Y_{12}), \quad G_{BE} = A \cdot (Y_{11} + Y_{12}),$$
$$A = \frac{Y_{11} + Y_{12} + Y_{21} + Y_{22}}{(1 - R_{BI}(Y_{11} + Y_{12}))(Y_{11} + Y_{21})} \tag{3}$$

From this data, C_{BED} and τ_D were calculated for each bias as follows:

$$C_{BED} = \frac{\mathrm{Im}(G_{BE})}{\omega} - C_{BEJ}, \quad \tau_D = -\frac{\arg(G_T)}{\omega}, \tag{4}$$

where C_{BEJ} is the base-emitter barrier capacitance. Extracted bias dependence of C_{BED} is shown in Fig. 6. In the active regime forward diffusion charge can be written as $\tau_F I_C$, where τ_F is the bias dependent forward transit time. In VBIC this dependence is:

$$\tau_F = TF \cdot (1 + QTF\, q_1) \cdot \left(1 + XTF \left(\frac{I_C}{I_C + ITF} \right)^2 e^{\frac{V_{BCi}}{1.44 VTF}} \right). \tag{5}$$

Parameter *QTF* accounts for base width modulation, which is negligible in HBT. Parameter *VTF* accounts for suppressed electron extraction by collector electric field as V_{BCi} increases. This is also hardly the case in HBT, so both *QTF* and *VTF* are omitted (set to zero) in this study. C_{BED} can therefore be expressed as:

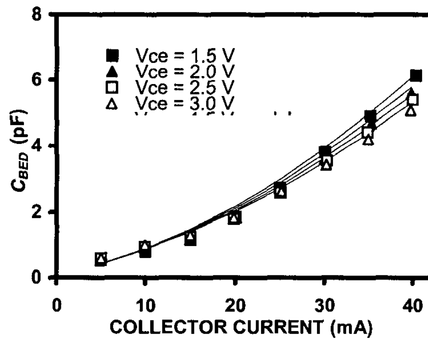

Fig. 6. Diffusion capacitance C_{BED} (symbols) extracted and (lines) calculated using (7). TF=2.5 ps, XTF = 6 and ITF = 100 mA.

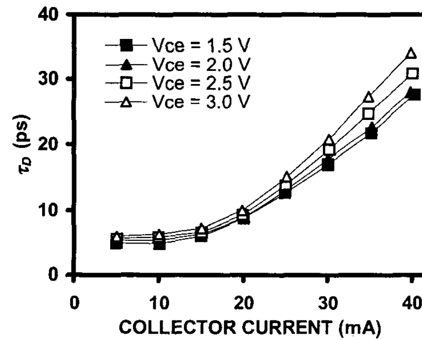

Fig. 7. Excess phase delay τ_D extracted according to Equation (4).

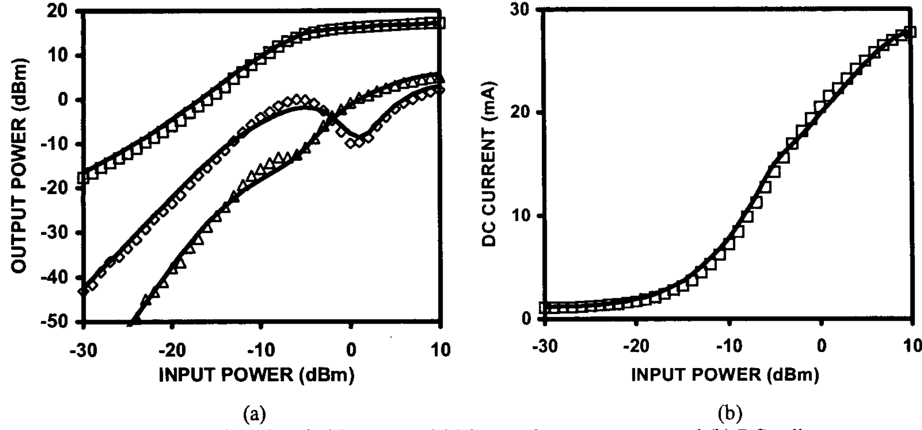

(a) (b)

Fig. 8. (lines) Simulated vs. (symbols) measured (a) harmonic output power and (b) DC collector current. Class B, 1 GHz, 125 Ω load, 1 mA quiescent current, 400 Ω bias resistor in series with base. (□) fundamental frequency at 1 GHz, (◇) 2nd, and (△) 3rd harmonics

$$C_{BED} = \frac{d(\tau_F I_C)}{d V_{BEi}} = G_m \cdot TF \cdot \left(1 + XTF \cdot \left(\frac{I_C}{I_C + ITF} \right)^2 \left(1 + \frac{2\,ITF}{I_C + ITF} \right) \right). \tag{6}$$

Here G_m is the DC transconductance $I_C/(n \cdot \varphi_T)$. Parameters TF, ITF and XTF were extracted by fitting (6) to C_{BED} from (4). Results of this extraction are also plotted in Fig. 6 confirming that (6) can be used to account for the Kirk effect.

Extracted bias dependence of τ_D is shown in Fig. 7. The dramatic increase of τ_D after onset of the Kirk effect is because of the way the transconductance is implemented in VBIC and the simplified model: $G_T = G_m \cdot e^{-j\omega\tau_D}$. Theoretically however this should be $G_T = G_m \, e^{-j\omega\tau_\varphi} / (1 + j\omega\tau_T)$, where τ_φ and τ_T are yet another bias-dependent time constants related to the collector transit time and base transit time, respectively. The overall phase shift $\omega \cdot \tau_D$ therefore equals to $\omega(\tau_\varphi + \tau_T)$, which explains enormous growth of τ_D in Fig. 7. Since there is no way to implement such bias dependence of τ_D in VBIC, the low-current τ_D~ 6 ps was selected as the model parameter *TD*.

The reverse transit time (parameter TR) in VBIC accounts for the charge of reverse transport electrons. However, in HBT this may not be the dominant charge when base-collector junction becomes forward biased. Calculations show that the charge of holes accounting for the non-ideal component of base-collector current is several orders of magnitude higher than that of reverse transport electrons. To account for this effect the charge sources $\tau_P \cdot I_{BCX2}$ and $\tau_P \cdot I_{BCI2}$ (where τ_P is the recombination time for holes in collector) connected in parallel with corresponding current sources are required. This is not possible in terms of VBIC model though. A possible workaround is to use reverse transport current component of I_{CC} to model $\tau_P \cdot I_{BCI2}$ and use reverse transport current component of I_{CCP} to model $\tau_P \cdot I_{BCX2}$. The substrate terminal in this case should be connected to the collector. This approach was implemented and *TR* was adjusted to fit large-signal data. Since reverse transport currents are usually smaller than I_{BCI2} and I_{BCX2}, the resulting value of parameter *TR* (~50 ns) significantly overestimates what is typically reported τ_P ~ 1 ns. Extracted VBIC model was verified against large-signal measurement as shown in Fig. 8.

5 Conclusion

In this work the key part of VBIC model was successfully extracted for InGaP/GaAs HBT. Throughout the extraction applicability of the model was analysed. It was found that, in spite of being unable to model non-linear thermal resistance, temperature dependent ideality factors and bias-

dependent excess phase delay, VBIC is suitable for InGaP/GaAs HBT modelling at least up to several GHz.

References

[1] C.C. McAndrew, J.A. Seitchik, D.F. Bowers, M. Dunn, M. Foisy, I. Getreu, M. McSwain, S. Moinian, J. Parker, D.J. Roulston, M. Shröter, P. van Wijnen, and L.F. Wagner, "VBIC95, the Vertivcal Bipolar Inter-Company Model," *IEEE Journal of Solid State Circuits*, Vol. 31, No 10, 1996.

[2] X. Cao, J. McMacken, K. Stiles, P. Laymen, J.J. Liou, A. Ortiz-Conde, S. Moinian, "Comparison of the New VBIC and Conventional Gommel-Poon Bipolar Transistor Models," *IEEE Trans. on Electron Devices,* Vol. 47, No. 2, pp. 427-433, 2000.

[3] M. Olavsbråten, "Parameter Extraction and Evaluation of the Bias Dependence of T_f, for the VBIC Model Used in GaAs HBT," *Proceedings of 2001 MTT-S International Microwave Simposium*, to be published.